HHS Public Access

Author manuscript

Nat Cell Biol. Author manuscript; available in PMC 2015 October 01.

Published in final edited form as:

Nat Cell Biol. 2015 April ; 17(4): 376–385. doi:10.1038/ncb3122.

Rapid Depot-Specific Activation of Adipocyte Precursor Cells at the Onset of Obesity

Elise Jeffery[1], **Christopher D. Church**[2], **Brandon Holtrup**[3], **Laura Colman**[2], and **Matthew S. Rodeheffer**[2,3,4,5]

[1]Yale University, Department of Cell Biology

[2]Section of Comparative Medicine

[3]Department of Molecular, Cell and Developmental Biology

[4]Yale Stem Cell Center

Abstract

Excessive accumulation of white adipose tissue (WAT) is the defining characteristic of obesity. WAT mass is composed primarily of mature adipocytes, which are generated through the proliferation and differentiation of adipocyte precursors (APs). While the production of new adipocytes contributes to WAT growth in obesity, little is known about the cellular and molecular mechanisms underlying adipogenesis in vivo. Here, we show that high-fat diet feeding in mice rapidly and transiently induces proliferation of APs within WAT to produce new adipocytes. Importantly, the activation of adipogenesis is specific to the perigonadal visceral depot in male mice, consistent with the patterns of obesogenic WAT growth observed in humans. Additionally, we find that in multiple models of obesity, the activation of APs is dependent upon the phosphoinositde 3-kinase (PI3K)-AKT2 pathway; however, the development of WAT does not require AKT2. These data indicate that developmental and obesogenic adipogenesis are regulated through distinct molecular mechanisms.

Introduction

The number of overweight and obese individuals continues to rise such that by the year 2030 it is projected that over half of the world's population will be overweight or obese[1]. Despite the defining role of white adipose tissue (WAT) accumulation in this disease, our understanding of WAT growth in obesity is limited. WAT can expand via both an increase in adipocyte size (hypertrophy) and adipocyte number (hyperplasia)[2–4], and recent studies

[5]Correspondence should be addressed to: Matt Rodeheffer, matthew.rodeheffer@yale.edu, Section of Comparative Medicine, Yale University School of Medicine, 375 Congress Ave, New Haven, CT 06520, Tel #203-737-3370, Fax #203-785-7499.

Author Contributions

E.J., C.D.C. and M.S.R. designed experiments. E.J., C.D.C., B.H., L.C. and M.S.R. performed experiments. E.J., C.D.C. and B.H. analyzed data. E.J., C.D.C., B.H. and M.S.R. interpreted data. E.J. and M.S.R. wrote the manuscript.

Competing Financial Interests Statement

The authors declare no competing financial interests.

have found that adipocyte hyperplasia plays an important role in human obesity[5,6]. Specifically, obese individuals have significantly more adipocytes than lean individuals, and this trend is maintained throughout adult life[5]. Even after obese individuals undergo severe weight loss, elevated adipocyte number is maintained[5], indicating that increased adipocyte formation in obesity has life-long effects on adipose tissue homeostasis and WAT mass. Another study found that variation in the size of the major omentum, a prominent visceral depot in humans, is primarily due to adipocyte number[6]. These data suggest that hyperplastic growth of WAT has important implications for metabolic health, given the risk of complications that accompany visceral obesity, including diabetes and cardiovascular disease[7–9]. Finally, several reports suggest that increased adipocyte number also contributes to obesity in rodents[10–14]. These studies point to a crucial role for adipocyte hyperplasia in the progression of obesity, yet the cellular and molecular mechanisms underlying the regulation of adipocyte number in vivo remain unclear.

Results

The hyperplastic growth of WAT requires the formation of new adipocytes in vivo. Since mature adipocytes are post-mitotic, new adipocytes arise from the differentiation of adipocyte precursor (AP) cells residing within the adipose tissue stromal-vascular fraction (SVF)[15,16]. Importantly, the timing of AP activation and subsequent adipogenesis remains undefined, and the molecular cues regulating this process in vivo are not known. To quantitatively assess the formation of adipocytes in response to high-fat diet (HFD) feeding in male C57BL/6J mice, we performed an adipocyte pulse-chase experiment using an adipocyte-specific, tamoxifen-inducible *Adiponectin-cre Estrogen Receptor* (*Adiponectin-creER*) mouse model[17] in combination with a dual fluorescent reporter. Upon expression of cre recombinase, the fluorescent reporter undergoes an indelible switch from expression of plasma membrane-targeted Tomato (mT, red fluorescence) to plasma membrane-targeted GFP expression (mG, green fluorescence) allowing for clear identification of cre-expressing cells[18,19]. Tamoxifen treatment results in approximately 95% recombination efficiency in the adipocytes of both the inguinal subcutaneous (SWAT) and perigonadal visceral (VWAT) adipose depots (Figure 1). To observe formation of new adipocytes, we pulsed *Adiponectin-cre ER; mT/mG* mice with tamoxifen and subsequently placed the mice on HFD for 8 weeks or continued mice on standard low-fat diet (SD). We then quantified the percentage of adipocytes labeled with mTomato, which indicates that they formed from mGFP-negative, mTomato-positive APs after the tamoxifen pulse (Figure 1A). We observe significantly increased formation of adipocytes exclusively in VWAT of HFD-fed male mice, while adipocyte formation is not enhanced by HFD in SWAT (Figure 1B–C). These data are consistent with recent qualitative findings using the Adipochaser mouse[13], which showed that new adipocytes form in male VWAT between 5 and 8 weeks of HFD feeding; however the timing of AP activation and adipogenesis in response to HFD is unknown.

In many adult tissues, cellular differentiation supports tissue homeostasis and expansion, and this process requires proliferation to maintain precursor pools[20]. Therefore, we reasoned that identifying the timing of AP proliferation in diet-induced obesity would allow us to determine when AP activation and subsequent differentiation is initiated. While increased proliferation of total SVF cells in WAT after long-term HFD feeding has been reported[21,22],

we focused on the first several weeks of HFD feeding to identify the cellular events that give rise to differentiated adipocytes by week 8 of HFD (Figure 1B–C). We investigated the proliferation of APs[16,19] in VWAT and SWAT depots by labeling with bromodeoxyuridine (BrdU) in vivo during a time course of HFD feeding in male mice (Supplementary Figure 1A). Flow cytometry analysis of BrdU incorporation into Lin^- :$CD29^+$:$CD34^+$:$Sca\text{-}1^+$ APs[23] (Figure 2A and Supplementary Figure 1B) shows increased proliferation of APs only in VWAT during the first week of HFD feeding (Figure 2B). The initial burst of AP proliferation is followed by a return to background proliferation rates by the second week of HFD and remains low throughout the remainder of the time course (Figure 2B). In contrast, we do not observe a significant increase in the proliferation of SWAT APs in response to HFD feeding (Figure2B).

We previously identified two subpopulations of APs, including Lin^- :$CD34^+$:$CD29^+$:$Sca\text{-}1^+$:$CD24^+$ ($CD24^+$) adipocyte progenitors and Lin^- :$CD34^+$:$CD29^+$:$Sca\text{-}1^+$:$CD24^-$ ($CD24^-$) committed preadipocytes[16,19]. After 1 week of BrdU treatment, these populations appear to proliferate at similar rates (Figure 2C–D); however, a shorter BrdU treatment of 12 hours reveals that AP proliferation is largely restricted to the $CD24^+$ adipocyte progenitor population in both major depots of HFD and SD-fed mice (Figure 2C–D). Given that activated $CD24^+$ adipocyte progenitors can rapidly differentiate into $CD24^-$ preadipocytes after only 24 hours[19,24], these data suggest that the increased proliferation of $CD24^+$ cells is masked during longer BrdU treatments by their rapid differentiation into $CD24^-$ cells. Since there is no difference in BrdU incorporation into the AP subpopulations with treatments longer than 12 hours, we performed all further analyses on the total AP population, which includes both the $CD24^+$ adipocyte progenitors and $CD24^-$ preadipocytes.

To verify that HFD-induced AP proliferation leads to an increase in the number of APs in VWAT, we utilized *PdgfRα-H2B*-GFP mice. These mice express a nuclear GFP reporter from the endogenous PdgfRα promoter, which labels primarily APs in WAT ([19,25] and Supplementary Figure 2C). As expected, proliferation of the GFP^+ cells in *PdgfRα-H2B*-GFP VWAT is significantly enhanced with HFD feeding (Supplementary Figure 2D). We used confocal microscopy to quantify total GFP^+ nuclei in situ and found that the number of $PdgfR\alpha^+$ cells nearly doubles in VWAT after 1 week of HFD compared to age-matched SD-fed controls (Figure 2E–F). These data indicate that a larger precursor pool is created within the WAT depot after only a short period of HFD feeding, which is consistent with the subsequent formation of new mature adipocytes over time (Figure 1B–C).

Next we determined when proliferative APs give rise to mature adipocytes during the expansion of WAT in diet-induced obesity. For these experiments we treated mice with BrdU during the first week of HFD feeding and used BrdU as a marker to track activated APs in vivo. We then placed the mice on HFD for different lengths of time and used two complementary quantitative methods to measure BrdU incorporation into mature adipocyte nuclei (Figure 3A). First, we isolated adipocyte nuclei by collagenase digestion and differential centrifugation after 1, 4, and 7 weeks of diet and performed flow cytometry analysis for BrdU. We find that after 1 and 4 weeks of diet there is no significant differentiation of activated APs into mature adipocytes; however after 7 weeks of diet we

detect BrdU labeling in mature adipocyte nuclei from all groups (Figure 3B). Importantly, the percentage of BrdU-positive adipocyte nuclei is significantly higher in the VWAT of HFD-fed mice compared to SD controls (Figure 3B), while there was no difference between SD- and HFD-fed groups in SWAT (Figure 3B). These results are consistent with the depot-specific AP proliferation pattern that we observe at the onset of HFD feeding. Interestingly, when we analyze BrdU labeling in the SVF after 7 weeks, we find a significant reduction in the percentage of BrdU-labeled APs in VWAT compared to the first week of HFD (Figure 3C), consistent with the hypothesis that a significant subset of BrdU-labeled APs transition from the SVF to the adipocyte pool during this time. Finally, BrdU pulse-chase from the second week of HFD-feeding (Supplementary Figure 2A), when AP proliferation has returned to SD levels (Figure 2B), shows no difference in the rate of mature adipocyte labeling between SD and HFD-fed groups (Supplementary Figure 2B).

The second method we used to measure the differentiation of activated APs was immunofluorescence staining of adipose tissue sections after 1 week of BrdU and 8 weeks of diet (Figure 3A). VWAT sections were stained for Caveolin-1 to identify adipocyte plasma membranes, and DAPI was used in combination with BrdU staining to assess BrdU incorporation into adipocyte nuclei (Figure 3D,[24]). Using this method, we find significantly increased adipocyte formation from proliferative cells in VWAT of HFD-fed mice (Figure 3D–E). Taken together, these data indicate that APs activated during the first week of HFD undergo adipogenesis to form new adipocytes in a depot-specific manner over a period of several weeks, thereby contributing to the expansion of fat mass at the onset of obesity.

Next, we determined the molecular pathways involved in HFD-induced AP activation. To further characterize the dynamics of AP proliferation in response to HFD, we treated groups of mice with BrdU for individual days at the onset of HFD-feeding. We found that AP proliferation in VWAT was highest at day 3 of HFD feeding and returned to SD levels by day 5 (Figure 4A). This surprisingly rapid activation of APs upon switching diets suggests that WAT cellular homeostasis is closely linked to nutrient sensing. One pathway that is involved in nutrient sensing mechanisms is the phosphoinositide 3-kinase (PI3K)-AKT pathway[26]. To determine whether the central kinase in this pathway, AKT, is activated in VWAT at the height of the proliferation response, we analyzed AKT phosphorylation at two critical activation sites[27] in the VWAT of mice after 3 days of HFD feeding. There is no significant increase in AKT phosphorylation in protein lysates from whole adipose tissue (Supplementary Figure 3A–B), which contains many cell types[28]. However, when we analyze APs by flow cytometry on day 3 of HFD feeding (Supplementary Figure 3C–D) we find that AKT phosphorylation at both sites is significantly elevated within APs in VWAT (Figure 4B–C). Furthermore, when we combine AKT phosphorylation analysis with BrdU labeling on the third day of diet, we find a significant positive correlation between AP proliferation rate and the level AKT phosphorylation in APs within VWAT (Figure 4D–E). When we perform the same analysis on day 14 of diet, when AP proliferation rates have returned to background levels, we observe no difference in AKT phosphorylation in APs between SD and HFD-fed groups (Figure 4F). These data indicate that AKT signaling within APs is correlated with AP proliferation and therefore may play a role in the activation of APs at the onset of obesity.

The AKT kinases regulate several processes including cellular growth, survival, and metabolism[29]. The most prominent mammalian isoforms are AKT1 and AKT2. While AKT1 is widely expressed and promotes the growth of many tissues[30,31], AKT2 regulates metabolic flux within liver, muscle, and, adipose tissue.[32,33]. Since AKT1 and AKT2 are both expressed in APs isolated from both VWAT and SWAT (Figure 5A), we isolated APs from VWAT after 3 days of HFD feeding and analyzed AKT1 and AKT2 phosphorylation by western blot. Using antibodies specific for phosphorylated AKT2 at S474 and AKT1 at S473, we find significant elevation of phospho-AKT2 at the height of AP activation in HFD-fed mice while levels of phospho-AKT1 are low in APs and do not increase in response to HFD (Figure 5B–C). We do, however, detect phospho-AKT1 in the non-AP cell population. (Supplementary Figure 3E). These data indicate that AKT2 is specifically activated in APs in response to HFD-feeding.

To test whether signaling through the PI3K pathway is required for AP activation upon HFD feeding, we performed daily injections of wortmannin, a PI3K inhibitor, during the first week of HFD feeding. This treatment blocks AP proliferation in VWAT (Figure 5D) with no effect on SWAT AP proliferation (Supplementary Figure 4A), indicating that PI3K signaling is required for HFD-induced AP activation. To focus our study on AKT2 signaling within adipose tissue, we generated a conditional knockout of AKT2 with the *PdgfRα* promoter, which targets adipocyte lineage cells[19], but not liver or muscle[17]. We find that full excision of the *Akt2* gene is achieved in APs from both SWAT and VWAT (Supplementary Figure 4B), and that *PdgfRα-cre; Akt2*$^{flox/flox}$ mice display normal body weight at 6 weeks of age (Supplementary Figure 4C). When we place these mice on HFD to assess the activation of APs, we find a significant reduction in AP proliferation in VWAT of *PdgfRα-cre; Akt2*$^{flox/flox}$ mice compared to HFD-fed controls (Figure 5E), despite normal food intake (Supplementary Figure 4D), while SWAT AP proliferation levels remain low in these mice (Supplementary Figure 4E). Additionally, BrdU pulse-chase analysis shows that after 8 weeks of HFD, adipocyte formation in VWAT of *PdgfRα-cre; Akt2*$^{flox/flox}$ mice is not increased compared to SD-fed wild-type mice (Figure 5F), indicating a lack of AP activation pogenesis. While the precise role response to HFD. These data show that AKT2 signaling within the adipocyte cellular lineage is required to support the activation of APs at the onset of HFD-induced obesity.

Consistent with the isoform-specific role of AKT2 in AP activation, AKT1 global knockout mice placed on HFD for 1 week display AP proliferation rates in VWAT similar to wild-type mice (Figure 6A), while mice lacking AKT2 display significantly reduced VWAT AP proliferation on HFD (Figure 6A); however, we observe no difference in SWAT proliferation rates (Figure 6B). When we analyze the production of new adipocytes in *Akt2*$^{-/-}$ mice by BrdU pulse labeling we find that, similar to *PdgfRα-cre; Akt2*$^{flox/flox}$ mice, there is no significant increase in the percentage of BrdU-labeled mature adipocytes in *Akt2*$^{-/-}$ HFD-fed mice compared to SD-fed mice (Figure 6C). These data indicate that AKT2 is indeed the AKT isoform required for AP activation in response to HFD feeding.

To determine whether the AKT2-dependent mechanism of adipocyte hyperplasia is restricted to HFD-induced obesity, we investigated the role of AKT2 in adipose tissue expansion of *ob/ob* mice, which lack functional leptin, exhibit hyperphagia, and become

extremely obese[34]. At weaning, *ob/ob; Akt2*$^{-/-}$ mice have similar body weight and fat mass to *ob/ob* mice (Figure 6D–E), and they display a hyperphagic phenotype whether measured as total calories (Supplementary Figure 5A) or calories normalized to body weight (Supplementary Figure 5B). During this period of hyperphagia, *ob/ob* mice display elevated rates of AP proliferation compared to wild-type mice, while *ob/ob; Akt2*$^{-/-}$ mice do not (Figure 6F), which indicates a defect in AP activation in the absence of AKT2. Although *ob/ob; Akt2*$^{-/-}$ mice also display reduced adipocyte hypertrophy compared to *ob/ob* mice (Supplementary Figure 5C–D), these data suggest that their reduced VWAT mass at 12 weeks of age (Figure 6G) is partially due to a defect in adipogenesis. Thus, AKT2 plays a role in AP activation at the onset of leptin-deficient obesity in addition to HFD-induced obesity.

Given the requirement for AKT2 in the obesogenic growth of WAT, we sought to determine whether AKT2 also plays a role in the normal growth of WAT by characterizing the development of WAT in wild-type and *Akt2*$^{-/-}$ mice. During the establishment of the SWAT depot prior to birth and the VWAT depot during the first week of postnatal life (Figure 7A and [35]), APs within these depots undergo robust proliferation (Figure 7B–C). This proliferation is followed by rapid hypertrophic growth of newly formed adipocytes[35,36] (Figure 7D–E and Supplementary Figure 6A–B). AP proliferation rates in both SWAT and VWAT do not differ between wild-type and *Akt2*$^{-/-}$ mice at any observed developmental time point (Figure 7B–C). Likewise, quantification of adipocyte size in both depots during development shows no difference in hypertrophic growth of adipocytes between wild-type and *Akt2*$^{-/-}$ mice (Figure 7D–E and Supplementary Figure 6A–B). Finally, total body fat mass upon weaning and into young adulthood is not significantly different between wild-type and *Akt2*$^{-/-}$ mice (Figure 7F), and *PdgfRα-cre; Akt2*$^{flox/flox}$ mice also have normal fat mass at 6 weeks of age (Supplementary Figure 6C), indicating that developmental WAT growth occurs normally in the absence of AKT2. Taken together, these data show that the regulation of adipogenesis occurs through distinct mechanisms in obesity and development.

Discussion

Although the formation of adipose tissue in development and the expansion of adipose tissue in obesity are often viewed as temporal variations on the same regulatory process, we show here that the formation of adipocytes in obesity and development are controlled by distinct molecular mechanisms. The existence of an aberrant mechanism of adipogenesis in obesity supports the American Medical Association's classification of obesity as a disease[37] and suggests that WAT regulation is more complex than previously appreciated. It has been hypothesized that once adipocytes reach their maximal size they stimulate the production of new adipocytes[11,14]. Our data show, however, that at the onset of diet-induced obesity, adipogenesis is initiated long before existing adipocytes reach their maximum lipid-filling capacity. Nonetheless, it is possible that signal(s) from hypertrophied adipocytes promote the subsequent lipid filling of activated APs, given that the maturation of these cells takes several weeks in vivo (Figure 3 and [13]).

We show here that AKT2 is required for the activation of APs in obesogenic adipogenesis. While the precise role of AKT2 in this process remains to be determined, AKT2 is known to

promote glucose uptake and insulin signaling within insulin-sensitive tissues such as liver, muscle and adipose[32,33]. C57BL/6 mice with global knockout of AKT2 develop normally but display a mild diabetic phenotype[32], and studies focused on liver metabolism have demonstrated that AKT2 is required for de novo lipogenesis[38]. Given that insulin signaling and lipogenesis play important roles in adipogenesis[39–41], it is possible that AKT2 functions to promote these pathways during AP activation. Additionally, in response to obesogenic stimuli, mice lacking AKT2 are protected from weight gain[38], which our data indicate is partially due to a deficiency in hyperplastic WAT growth. Previous studies have also suggested that AKT2 is involved in regulating WAT mass in humans. Specifically, a dominant negative *Akt2* allele results in reduced WAT mass[42], while an activating *Akt2* mutation is associated with excess WAT accumulation[43]. Data presented here, combined with the recent finding that human VWAT expansion is primarily controlled by adipocyte hyperplasia[6], suggest that AKT2 plays a role in the expansion of WAT through increased adipocyte number in human obesity.

Our data also have important implications for the understanding of obesity-related disease. The accumulation of VWAT is associated with higher risk of obesity-related diseases such as diabetes, cardiovascular disease, and cancer[7–9]. Conversely, the accumulation of SWAT may have beneficial effects on glucose homeostasis[44,45]. In combination with the findings presented here, these data suggest that the metabolic consequences associated with visceral obesity may be linked to hyperplastic expansion in this depot. While several studies have examined differences between subcutaneous and visceral adipose tissue, often focusing on gene expression[46,47], metabolic activity[44,45,48], or cellular lineage[49,50], it remains unclear which feature(s) of the VWAT is responsible for the selective activation of visceral APs in HFD-induced obesity. The new adipocytes formed via obesogenic adipogenesis may have altered function, and thus directly contribute to endocrine dysfunction or inflammation in WAT. Alternatively, the production of more adipocytes may be beneficial, increasing the capacity of WAT to store excess lipid, thereby decreasing ectopic lipid accumulation in other tissues, which can promote metabolic disease[51,52].

This study provides a framework for understanding the effects of dietary nutrient sensing on cellular mechanisms of tissue homeostasis. Our data suggest that even relatively short binges of altered eating behavior may stimulate obesogenic adipogenesis, resulting in an intractable increase in adipocyte number[5] that may make future weight loss more difficult. Future studies will determine the long-term effect of this transient induction of adipogenesis on adipocyte number, weight gain, and metabolic disease. Finally, identification of the precise nutrient signal(s) involved may lead to the development of therapeutic strategies to target the obesity-specific pathway, ameliorating WAT gain in human obesity without affecting normal WAT mass.

Materials and Methods

Animals

All animal studies followed guidelines issued by Yale University's Institutional Animal Care and Use Committee (IACUC). All mice used for these studies were on the C57BL/6J genetic background. Adult wild type mice were purchased from Jackson Laboratories. When

possible, mice were randomized based on body weight to achieve similar average weight in different groups. For experiments involving developmental time points, wild type mice were purchased from Jackson Laboratories and bred in the Yale Animal Resource center. Akt2−/− and Akt1−/− mice were a generous gift from Dr. William Sessa, Yale University. Akt2$^{flox/flox}$ mice were a generous gift from Dr. Morris Birnbaum, (University of Pennsylvania) via Kathleen Martin (Yale University), and Adiponectin-CreER mice were a generous gift from Dr. Evan Rosen (Beth Israel Deaconess Medical Center, Boston, MA) and can now be purchased at Jackson Laboratories (stock no. 024671). For adipocyte pulse chase experiments, mT/mG B6.129(Cg)-Gt(ROSA)26Sortm4(ACTB-tdTomato,-EGFP)Luo/J), stock no. 007676 were purchased from Jackson Laboratories and bred to Adiponectin-CreER mice in the Yale Animal Resource Center. PdgfRα-Cre mice (stock no. 013148) were purchased from Jackson Laboratories. PdgfRα-H2B-GFP mice, stock no. 007669, were purchased from Jackson Labs and bred in the Yale Animal Resource Center. Unless otherwise noted, mice were males 6–8 weeks of age at the start of experiments. In this study VWAT refers to the perigonadal visceral adipose tissue in mice. SWAT refers to inguinal subcutaneous adipose tissue in mice. For BrdU (US Biological, B2850) treatments lasting 12–24 hours, mice or pregnant mothers were given intraperitoneal injections of 50 mg/kg BrdU in sterile PBS every 6 hours. For BrdU treatments lasting longer than 24 hours, BrdU was administered in the drinking water at 0.8mg/mL for experiments lasting 1 week or less, or 0.4mg/mL for experiments lasting longer than 1 week. BrdU water was refreshed every 2 days. Where indicated, mice were given daily intraperitoneal injections of freshly-made Wortmannin (1mg/kg, Cayman Chemical, 10010591) in 1:8 DMSO:PBS. High fat diet is from Research Diets (D12492). Standard diet is from Harlan Laboratories (2018S).

Flow cytometry analysis of cell proliferation

Isolation of adipose tissue stromal cells was performed as described[23]. Briefly, adipose tissue was excised, minced, and digested in Hank's Balanced Salt Solution (HBSS) (Sigma #H8264) containing 3% BSA and 0.8 mg/mL Collagenase Type 2 (Worthington Biochemical; LS004174) for 75 minutes in a shaking water bath at 37°C. The mixture was then filtered through a 40μm filter, and filtered cells were pelleted and washed in HBSS containing 3% BSA. For BrdU analysis, cells were stained with the following antibodies: CD45 APC-eFluor 780 (eBioscience; 47-0451-80, clone 30-F11, used at 1-5000), CD31 PE-Cy7 (eBioscience, 25-0311-82, clone 390, used at 1–1000), CD29 Alexa Fluor 700 (BioLegend, 102218, used at 1–400) and Sca-1 Pacific Blue (BD Biosciences, 560653, clone D7, used at 1–400) or Sca-1 V500 (BD Horizon, 561228, clone D7, used at 1–250). Cells were washed, fixed and permeabilized using Phosflow lyse/fix and Perm Buffer III (BD Biosciences) according to the manufacturer's recommendations. Cells were then treated with DNase (deoxyribonuclease I; Worthington; × 6000 units/ml) in dPBS (Sigma; with calcium chloride and magnesium chloride) for 2 hours in a 37°C water bath and then washed in HBSS with 3% BSA. Cells were then stained with anti-BrdU antibody (Alexa Fluor 488; Phoenix Flow Systems; AX488 or Alexa Fluor 647; Phoenix Flow Systems; AX647, clone PRB-1, used at 1–35) in HBSS with 3% BSA overnight in the dark at 4°C. Cells were then washed in HBSS with 3% BSA and incubated with CD34 Alexa Fluor 647 (BioLegend, 119314, clone MEC14.7 used at 1–400) or CD34 Brilliant Violet 421 (BioLegend 119321, clone MEC14.7, used at 1–300), and CD24 PerCP-Cyanine 5.5 (eBioscience, 45-0242-80,

clone M1/69, used at 1–400). Following antibody incubation, samples were washed and analyzed on a BD LSRII analyzer. Data analysis was performed using BD FACS Diva software (BD Biosciences).

Analysis of phosphorylated Akt by flow cytometry

AP cells were isolated as described above[23], however all buffers used prior to fixation contained Roche PhosStop phosphatase inhibitor cocktail and 15 μM wortmannin (Cayman Chemical) to limit changes in pathway activation during isolation. Cells were fixed in BD Phosflow Lyse/Fix Buffer (BD Biosciences) and membranes were permeabilized in BD Phosflow Perm Buffer III (BD Biosciences) according to the manufacturer's instructions. Cells were stained for p-Akt with the following antibodies from Cell Signaling phospho-AKT S473 PE conjugate (#5315, clone D9E, used at 1–100) and phopho-AKT T308 PE conjugate (#9088, clone C31E5E, used at 1–100), at 4°C overnight. As a control for the ability of this isolation procedure to maintain the phosphorylation status of AKT, WAT was excised, minced and treated with varying concentrations of insulin in PBS at 37°C for 10 minutes, briefly washed to remove insulin, and AP cells were then isolated from the minced tissue as described above. Phospho-AKT staining with both antibodies displayed an appropriate dose-response pattern for different treatments (See Supplementary Figure 2C–D). For BrdU and p-AKT co-stain experiments, mice were treated for 12 hours with BrdU on the third night of HFD feeding, and then sacrificed.

Isolation of AP cells by bead separation

SVF cells were isolated as described above for analysis of phosphorylated AKT, and enrichment for AP cells was achieved using the EasySep Mouse PE Positive Selection Kit (Stem Cell Technologies #18554) using a Sca-1-PE antibody (eBioscience #12-5981-81) according to the manufacturer's instructions. Positively selected cells were then lysed on ice in 1% IGEPAL with protease inhibitors (Roche) and PhosStop phosphatase inhibitors (Roche). Protein concentration for the resulting lysates was determined using the BCA (bicinchoninic acid) Protein Assay kit from Pierce, and lysates were run on 10% polyacrylamide gels from Invitrogen, followed by western blotting analysis.

Isolation of adipocyte nuclei

Adipose tissue was minced into approximately 3–4mm pieces and gently digested in 1 mg/ml collagenase type 2 (Worthington Biochemical; LS004174) in Krebs Ringer Phosphate Buffer (KRP) for 80 minutes. Floating adipocytes were separated from stromal cells by centrifugation at 150g for 8 min, filtered through a 190 μm filter, and washed in KRP. Isolation of intact adipocytes was verified by staining for plasma membrane with Cell Mask Orange (Invitrogen, C10045) and nuclei with DAPI as described[23]. Adipocytes were lysed for 5 minutes in 0.2% IGEPAL in KRP with vortexing every 1–2 minutes. Adipocyte nuclei were isolated by centrifugation at 2000g for 5 minutes. For BrdU analysis, nuclei were fixed, permeabilized, and treated with DNAse and stained for BrdU as described above for stromal cells. For identification, nuclei were stained with propidium iodide and analyzed for BrdU incorporation on a BD LSRII analyzer. Data is shown as the percent of Propidium-positive events that were also BrdU-positive. Data analysis was performed using BD FACS Diva software (BD Biosciences).

Adiponectin-CreER; mT/mG pulse chase

Starting at 8 weeks of age, mice were treated with 50mg/kg tamoxifen (Sigma) dissolved in vegetable oil by intraperitoneal injection for 5 consecutive days, and then allowed to recover for 1 week. Mice were then sacrificed for baseline analysis, or placed on HFD or remained on SD for the 8-week chase period. Inguinal subcutaneous and perigonadal visceral tissue were taken from several regions throughout the depot, and analyzed by whole mount confocal microscopy for tdTomato and eGFP expression. For each data point, at least 150 (SWAT) or 1300 (VWAT) adipocytes were counted from multiple images from each depot of each animal.

Immunofluorescence

Adipose tissue was prepared as described for paraffin-embedded tissue[53]. Briefly, tissue was fixed in 1x zinc formaldehyde for 24–48 hours at 4°C, then washed with PBS. Samples were then dehydrated in increasing concentrations of ethanol over 6 hours, and embedded in paraffin wax. 5 μm sections of paraffin blocks were then deparaffinized and rehydrated, followed by antigen retrieval in 10mM sodium citrate, pH 6.0 under pressure in a 2100 Retriever (PickCell Laboratories). Blocking and staining was performed in 2% BSA in PBS. Sections were incubated in primary antibodies including rat anti-BrdU (Abcam #ab6326, clone # BU1/75 (ICR1) used at 1–350) and rabbit anti-Caveolin-1 (Cell Signaling #3238, used at 1–400) overnight at 4°C. Secondary antibodies including goat anti-rat-A488 (#112-545-167) and goat anti-rabbit rhodamine-X-red (#111-295-144), both used at 1–250, were purchased from Jackson Immunoresearch, and incubated with tissue for 1–2 hours at room temperature. Slides were mounted with DAPI Fluoromount-G mounting media (Southern Biotech) and imaged by confocal microscopy. Several confocal images of each tissue section were acquired, and analyzed for the presence of BrdU and adipocyte nuclei. Adipocyte nuclei were identified by their location inside adipocyte membranes as described[24].

Confocal Microscopy

For mT/mG quantification experiments, confocal microscopy was performed as described previously[19]. For developmental experiments, adipose tissue was excised and stained with HCS LipidTOX Green Neutral Lipid Stain (Invitrogen, H34475, used at 1–100) and Isolectin GS-IB4 Alexa 647 (Invitrogen, I32450, used at 1–200) for at least 30 minutes before being washed in PBS and mounted onto slides in Fluoromount-G (Southern Biotech; 0100-01). Images were taken on a Leica TCS SP5 confocal microscope. Size analysis of lipid droplets in developing WAT was performed on confocal images using Image J software.

For quantification of PdgfRα-positive nuclei in PdgfRα-H2B-GFP WAT, adult mice were either maintained on standard chow diet or fed high-fat diet for one week. GWAT was excised, weighed, and confocal z-stacks were taken on a Leica TCS SP5 confocal microscope. A representative 3D image taken from a z-stack is shown in Figure 2E. The nuclei were counted in ImageJ using the Object Counter3D (http://rsb.info.nih.gov/ij/plugins/track/objects.html) plugin. The volume of each z-stack was calculated using the dimensions of the stack (length: 387μm × width: 387μm × height: 0.7μm × number of

slices). Using the density of triolene (0.915 g/mL[7]) with the volume of each z-stack, the weight of each z-stack was calculated. Then, the average number of cells per gram was calculated using the total number of PdgfRα-positive nuclei in the stack and the weight of the z-stack. Lastly, the total number of cells in the depot was estimated by multiplying the number of cells per gram by the weight of each fat pad. Five animals were used in the control group (SD), and five animals were used in the experimental group (HFD). For each animal, a total of six z-stacks (50–250 virtual slices per z-stack) were created from multiple regions throughout the depot.

Food Intake and Body Composition

Analysis of body composition was performed by NMR using the Echo MRI whole body composition analyzer (Echo Medical System, Houston, TX). For food intake experiments with *ob/ob* animals, mice were individually caged and food and mice were weighed weekly. Kilocalories of food intake were normalized to the average body weight of the mouse at the beginning and end of the week. For *PdgfRα-cre; Akt2*$^{flox/flox}$ experiments, mice were individually caged and food intake was measured with a TSE PhenoMaster System for small laboratory animals. Kilocalories of food intake were normalized to the average body weight of the mouse at the beginning and end of the 4-day period.

Western blotting

Isolated AP cells were lysed in 1% IGEPAL with protease inhibitors (Roche) and PhosStop phosphatase inhibitors (Roche). Whole fat was snap frozen in liquid nitrogen, and homogenized on ice in RIPA buffer including 10% glycerol, 1% triton-X100, 0.1%SDS, 0.5% sodium deoxycholate, protease inhibitors (Roche) and PhosStop phosphatase inhibitors (Roche). Lysates were centrifuged at 4°C at 13,000 rpm and the lysate was transferred twice to remove lipid. Quantification of protein was performed using the BCA (bicinchoninic acid) Protein Assay kit from Pierce, and lysates were run on 10% polyacrylamide gels from Invitrogen. Protein was transferred to PVDF membrane using the Invitrogen NuPage system. Primary antibodies were purchased from Cell Signaling including rabbit anti-AKT1 (#2938, clone C73H10 used at 1–1000), rabbit anti-AKT2 (#3063, clone D6G4, used at 1–1000), rabbit anti-phospho-AKT1 S473 (#9018, clone D7F10, used at 1–500), rabbit anti-phospho-AKT2 S474 (#8599, clone D3H2, used at 1–500), rabbit anti-β actin (#4970, clone 13E5, used at 1–2000), and were diluted in tris-buffered saline with 0.1% Tween-20. Goat anti-rabbit-HRP secondary antibody was purchased from Jackson Immunoresearch (#211-032-171) and used at 1–10,000. Blots were developed using the SuperSignal West Pico Chemiluminescent Substrate from Pierce. Quantification was performed using Adobe Photoshop CS6. For experiments in which both phospho-AKT and total AKT were analyzed from the same blot, phospho-AKT was probed for first. The blot was then stripped with Thermo Scientific Restore Plus Western Blot Stripping Buffer for 5–10 minutes, washed, and incubated with secondary antibody for 30 minutes. The blot was then developed to check that there was no residual signal from phospho-AKT antibodies. The blot was then washed, and incubated in blocking buffer, and incubated with antibodies to detect total AKT.

Statistical analysis

Statistical tests used are indicated in the figure legends. All statistical tests were performed using GraphPad Prism version 6.02 for Windows (GraphPad Software). The investigators were not blinded to allocation during experiments and outcome assignment. Mice were genotyped prior to performing experiments. Data are expressed as mean ± SEM, and $P < 0.05$ was considered statistically significant. Samples were excluded from experiments if animals were not eating or were otherwise deemed unhealthy. Groups of at least 5 mice were used for experiments, unless statistical significance was reached with fewer animals. No statistical method was used to pre-determine sample size. Sample sizes for each group are listed in figure legends, and indicate individual animals (biological replicates).

Supplementary Material

Refer to Web version on PubMed Central for supplementary material.

Acknowledgments

This work was supported by American Diabetes Association Award 7-12-JF-46, DERC pilot project grant DK045735 and NIDDK grant DK090489 to M.S.R., Lo Graduate Fellowship for Excellence in Stem Cell Research from the Yale Stem Cell Center to E.J., and EMBO long-term fellowship ALTF 132-2011 to C.D.C.

References

1. Kelly T, Yang W, Chen CS, Reynolds K, He J. Global burden of obesity in 2005 and projections to 2030. Int J Obes (Lond). Sep; 2008 32(9):1431–1437. [PubMed: 18607383]
2. Peckham SC, Entenman C, Carroll HW. The influence of a hypercalric diet on gross body and adipose tissue composition in the rat. J Nutr. Jun.1962 77:187–197. [PubMed: 14484832]
3. Steinberg MD, Zingg W, Angel A. Studies of the number and volume of fat cells in adipose tissue. J Pediatr. Aug.1962 61:299–300. [PubMed: 13916686]
4. Enesco M, Leblond CP. Increase in Cell Number as a Factor in the Growth of the Organs and Tissues of the Young Male Rat. Journal of Embryology and Experimental Morphology. Dec 1; 1962 10(4):530–562.
5. Spalding KL, Arner E, Westermark PO, et al. Dynamics of fat cell turnover in humans. Nature. Jun 5; 2008 453(7196):783–787. [PubMed: 18454136]
6. Arner P, Andersson DP, Thorne A, et al. Variations in the size of the major omentum are primarily determined by fat cell number. J Clin Endocrinol Metab. May; 2013 98(5):E897–901. [PubMed: 23543656]
7. Phillips LK, Prins JB. The link between abdominal obesity and the metabolic syndrome. Curr Hypertens Rep. Apr; 2008 10(2):156–164. [PubMed: 18474184]
8. Bjorntorp P. Metabolic difference between visceral fat and subcutaneous abdominal fat. Diabetes Metab. Jun; 2000 26 (Suppl 3):10–12. [PubMed: 10945144]
9. Wang Y, Rimm EB, Stampfer MJ, Willett WC, Hu FB. Comparison of abdominal adiposity and overall obesity in predicting risk of type 2 diabetes among men. Am J Clin Nutr. Mar; 2005 81(3): 555–563. [PubMed: 15755822]
10. Hirsch J, Batchelor B. Adipose tissue cellularity in human obesity. Clin Endocrinol Metab. Jul; 1976 5(2):299–311. [PubMed: 1085232]
11. Faust IM, Johnson PR, Stern JS, Hirsch J. Diet-induced adipocyte number increase in adult rats: a new model of obesity. Am J Physiol. Sep; 1978 235(3):E279–286. [PubMed: 696822]
12. Lemonnier D. Effect of age, sex, and sites on the cellularity of the adipose tissue in mice and rats rendered obese by a high-fat diet. J Clin Invest. Nov; 1972 51(11):2907–2915. [PubMed: 5080416]

13. Wang QA, Tao C, Gupta RK, Scherer PE. Tracking adipogenesis during white adipose tissue development, expansion and regeneration. Nat Med. Oct; 2013 19(10):1338–1344. [PubMed: 23995282]
14. Cleary MP, Brasel JA, Greenwood MR. Developmental changes in thymidine kinase, DNA, and fat cellularity in Zucker rats. Am J Physiol. May; 1979 236(5):E508–513. [PubMed: 443370]
15. Cristancho AG, Lazar MA. Forming functional fat: a growing understanding of adipocyte differentiation. Nat Rev Mol Cell Biol. Nov; 2011 12(11):722–734. [PubMed: 21952300]
16. Rodeheffer MS, Birsoy K, Friedman JM. Identification of white adipocyte progenitor cells in vivo. Cell. Oct 17; 2008 135(2):240–249. [PubMed: 18835024]
17. Jeffery E, Berry R, Church CD, et al. Characterization of Cre recombinase models for the study of adipose tissue. Adipocyte. Jul 1; 2014 3(3):206–211. [PubMed: 25068087]
18. Muzumdar MD, Tasic B, Miyamichi K, Li L, Luo L. A global double-fluorescent Cre reporter mouse. Genesis. Sep; 2007 45(9):593–605. [PubMed: 17868096]
19. Berry R, Rodeheffer MS. Characterization of the adipocyte cellular lineage in vivo. Nat Cell Biol. Feb 24.2013
20. Pellettieri J, Sanchez Alvarado A. Cell turnover and adult tissue homeostasis: from humans to planarians. Annu Rev Genet. 2007; 41:83–105. [PubMed: 18076325]
21. Joe AW, Yi L, Even Y, Vogl AW, Rossi FM. Depot-specific differences in adipogenic progenitor abundance and proliferative response to high-fat diet. Stem Cells. Oct; 2009 27(10):2563–2570. [PubMed: 19658193]
22. Hudak CS, Gulyaeva O, Wang Y, et al. Pref-1 marks very early mesenchymal precursors required for adipose tissue development and expansion. Cell Rep. Aug 7; 2014 8(3):678–687. [PubMed: 25088414]
23. Church CD, Berry R, Rodeheffer MS. Isolation and study of adipocyte precursors. Methods Enzymol. 2014; 537:31–46. [PubMed: 24480340]
24. Berry R, Jeffery E, Rodeheffer MS. Weighing in on adipocyte precursors. Cell Metab. Jan 7; 2014 19(1):8–20. [PubMed: 24239569]
25. Lee YH, Petkova AP, Mottillo EP, Granneman JG. In vivo identification of bipotential adipocyte progenitors recruited by beta3-adrenoceptor activation and high-fat feeding. Cell Metab. Apr 4; 2012 15(4):480–491. [PubMed: 22482730]
26. Hietakangas V, Cohen SM. Regulation of tissue growth through nutrient sensing. Annu Rev Genet. 2009; 43:389–410. [PubMed: 19694515]
27. Pearce LR, Komander D, Alessi DR. The nuts and bolts of AGC protein kinases. Nat Rev Mol Cell Biol. Jan; 2010 11(1):9–22. [PubMed: 20027184]
28. Eto H, Suga H, Matsumoto D, et al. Characterization of structure and cellular components of aspirated and excised adipose tissue. Plast Reconstr Surg. Oct; 2009 124(4):1087–1097. [PubMed: 19935292]
29. Gonzalez E, McGraw TE. The Akt kinases: isoform specificity in metabolism and cancer. Cell Cycle. Aug 15; 2009 8(16):2502–2508. [PubMed: 19597332]
30. Cho H, Thorvaldsen JL, Chu Q, Feng F, Birnbaum MJ. Akt1/PKBalpha is required for normal growth but dispensable for maintenance of glucose homeostasis in mice. J Biol Chem. Oct 19; 2001 276(42):38349–38352. [PubMed: 11533044]
31. Chen WS, Xu PZ, Gottlob K, et al. Growth retardation and increased apoptosis in mice with homozygous disruption of the Akt1 gene. Genes Dev. Sep 1; 2001 15(17):2203–2208. [PubMed: 11544177]
32. Cho H, Mu J, Kim JK, et al. Insulin resistance and a diabetes mellitus-like syndrome in mice lacking the protein kinase Akt2 (PKB beta). Science. Jun 1; 2001 292(5522):1728–1731. [PubMed: 11387480]
33. Garofalo RS, Orena SJ, Rafidi K, et al. Severe diabetes, age-dependent loss of adipose tissue, and mild growth deficiency in mice lacking Akt2/PKB beta. J Clin Invest. Jul; 2003 112(2):197–208. [PubMed: 12843127]
34. Gautron L, Elmquist JK. Sixteen years and counting: an update on leptin in energy balance. J Clin Invest. Jun; 2011 121(6):2087–2093. [PubMed: 21633176]

35. Han J, Lee JE, Jin J, et al. The spatiotemporal development of adipose tissue. Development. Nov; 2011 138(22):5027–5037. [PubMed: 22028034]
36. Birsoy K, Berry R, Wang T, et al. Analysis of gene networks in white adipose tissue development reveals a role for ETS2 in adipogenesis. Development. Nov; 2011 138(21):4709–4719. [PubMed: 21989915]
37. Pollack, A. [Accessed January 12, 2015] AMA Recognizes Obesity as a Disease. [Internet]. 2013; http://www.nytimes.com/2013/06/19/business/ama-recognizes-obesity-as-a-disease.html
38. Leavens KF, Easton RM, Shulman GI, Previs SF, Birnbaum MJ. Akt2 is required for hepatic lipid accumulation in models of insulin resistance. Cell Metab. Nov; 2009 10(5):405–418. [PubMed: 19883618]
39. Czech MP, Tencerova M, Pedersen DJ, Aouadi M. Insulin signalling mechanisms for triacylglycerol storage. Diabetologia. May; 2013 56(5):949–964. [PubMed: 23443243]
40. Tontonoz P, Spiegelman BM. Fat and beyond: the diverse biology of PPARgamma. Annu Rev Biochem. 2008; 77:289–312. [PubMed: 18518822]
41. Lodhi IJ, Yin L, Jensen-Urstad AP, et al. Inhibiting adipose tissue lipogenesis reprograms thermogenesis and PPARgamma activation to decrease diet-induced obesity. Cell Metab. Aug 8; 2012 16(2):189–201. [PubMed: 22863804]
42. George S, Rochford JJ, Wolfrum C, et al. A family with severe insulin resistance and diabetes due to a mutation in AKT2. Science. May 28; 2004 304(5675):1325–1328. [PubMed: 15166380]
43. Hussain K, Challis B, Rocha N, et al. An activating mutation of AKT2 and human hypoglycemia. Science. Oct 28.2011 334(6055):474. [PubMed: 21979934]
44. Tran TT, Yamamoto Y, Gesta S, Kahn CR. Beneficial effects of subcutaneous fat transplantation on metabolism. Cell Metab. May; 2008 7(5):410–420. [PubMed: 18460332]
45. Wajchenberg BL. Subcutaneous and visceral adipose tissue: their relation to the metabolic syndrome. Endocr Rev. Dec; 2000 21(6):697–738. [PubMed: 11133069]
46. Yamamoto Y, Gesta S, Lee KY, Tran TT, Saadatirad P, Kahn CR. Adipose depots possess unique developmental gene signatures. Obesity (Silver Spring). May; 2010 18(5):872–878. [PubMed: 20111017]
47. Grove KL, Fried SK, Greenberg AS, Xiao XQ, Clegg DJ. A microarray analysis of sexual dimorphism of adipose tissues in high-fat-diet-induced obese mice. Int J Obes (Lond). Jun; 2010 34(6):989–1000. [PubMed: 20157318]
48. Macotela Y, Boucher J, Tran TT, Kahn CR. Sex and depot differences in adipocyte insulin sensitivity and glucose metabolism. Diabetes. Apr; 2009 58(4):803–812. [PubMed: 19136652]
49. Chau YY, Bandiera R, Serrels A, et al. Visceral and subcutaneous fat have different origins and evidence supports a mesothelial source. Nat Cell Biol. Apr; 2014 16(4):367–375. [PubMed: 24609269]
50. Krueger KC, Costa MJ, Du H, Feldman BJ. Characterization of cre recombinase activity for in vivo targeting of adipocyte precursor cells. Stem Cell Reports. Dec 9; 2014 3(6):1147–1158. [PubMed: 25458893]
51. Rosen ED, Spiegelman BM. What we talk about when we talk about fat. Cell. Jan 16; 2014 156(1–2):20–44. [PubMed: 24439368]
52. van Herpen NA, Schrauwen-Hinderling VB. Lipid accumulation in non-adipose tissue and lipotoxicity. Physiol Behav. May 23; 2008 94(2):231–241. [PubMed: 18222498]
53. Berry R, Church CD, Gericke MT, Jeffery E, Colman L, Rodeheffer MS. Imaging of adipose tissue. Methods Enzymol. 2014; 537:47–73. [PubMed: 24480341]

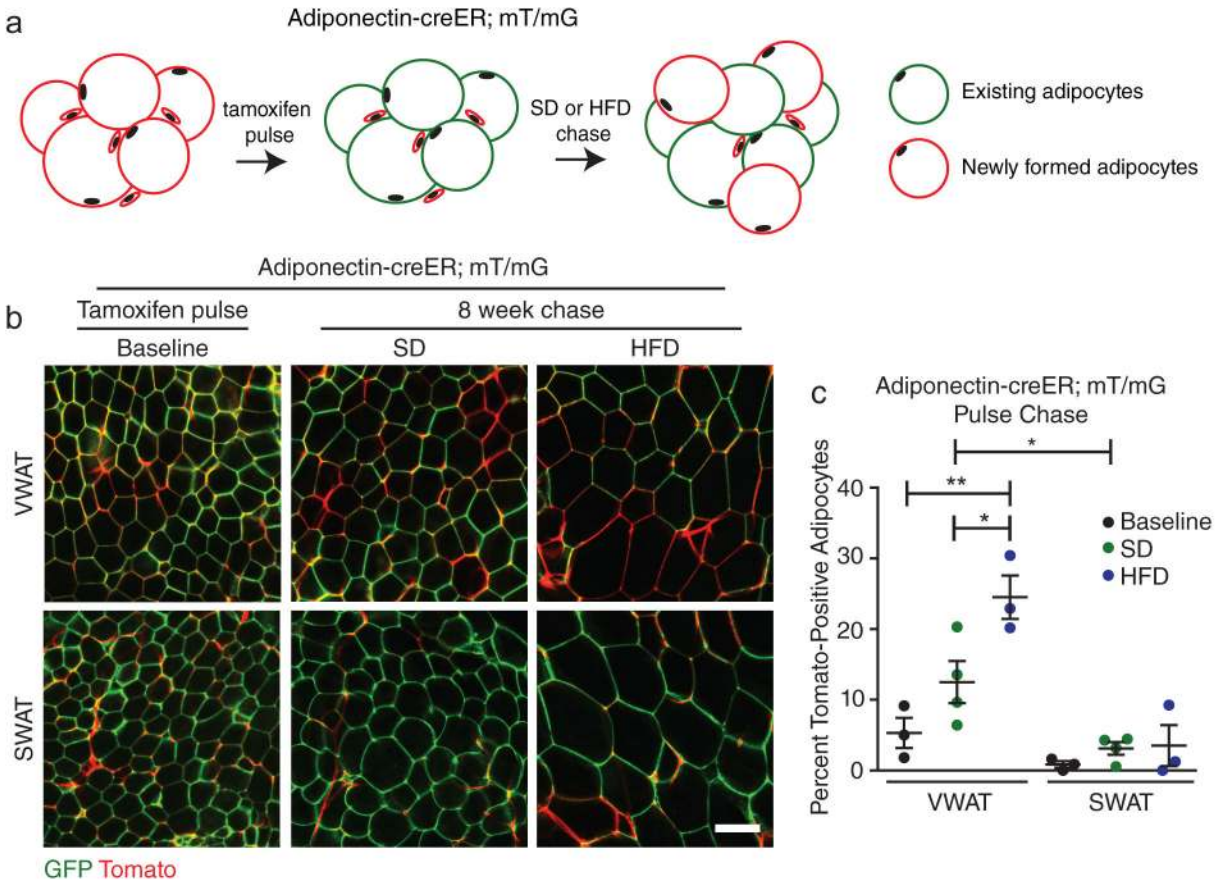

Figure 1. High-fat diet feeding induces depot-specific adipocyte hyperplasia

(**A**) Experimental scheme for analysis of in vivo adipogenesis with the *Adiponectin-creER; mT/mG* mouse model. (**B–C**) Representative images (B) and quantification (C) of adipocyte tracing in *Adiponectin-creER; mT/mG* mice after tamoxifen treatment followed by 8 weeks on the indicated diets (n = 3 mice for baseline and HFD, n = 4 mice for SD). Note that the vasculature remains mTomato-positive in the images in (B). Significance between the indicated groups in (C) was calculated using a two-tailed student's t-test. Exact p-values are listed in Supplementary Table 1. Error bars represent mean ± s.e.m. * (P<0.05), ** (p<0.01). Scale bar in (B) is 100μm. HFD: high-fat diet, SD: standard diet, mT/mG: membrane tomato/ membrane GFP.

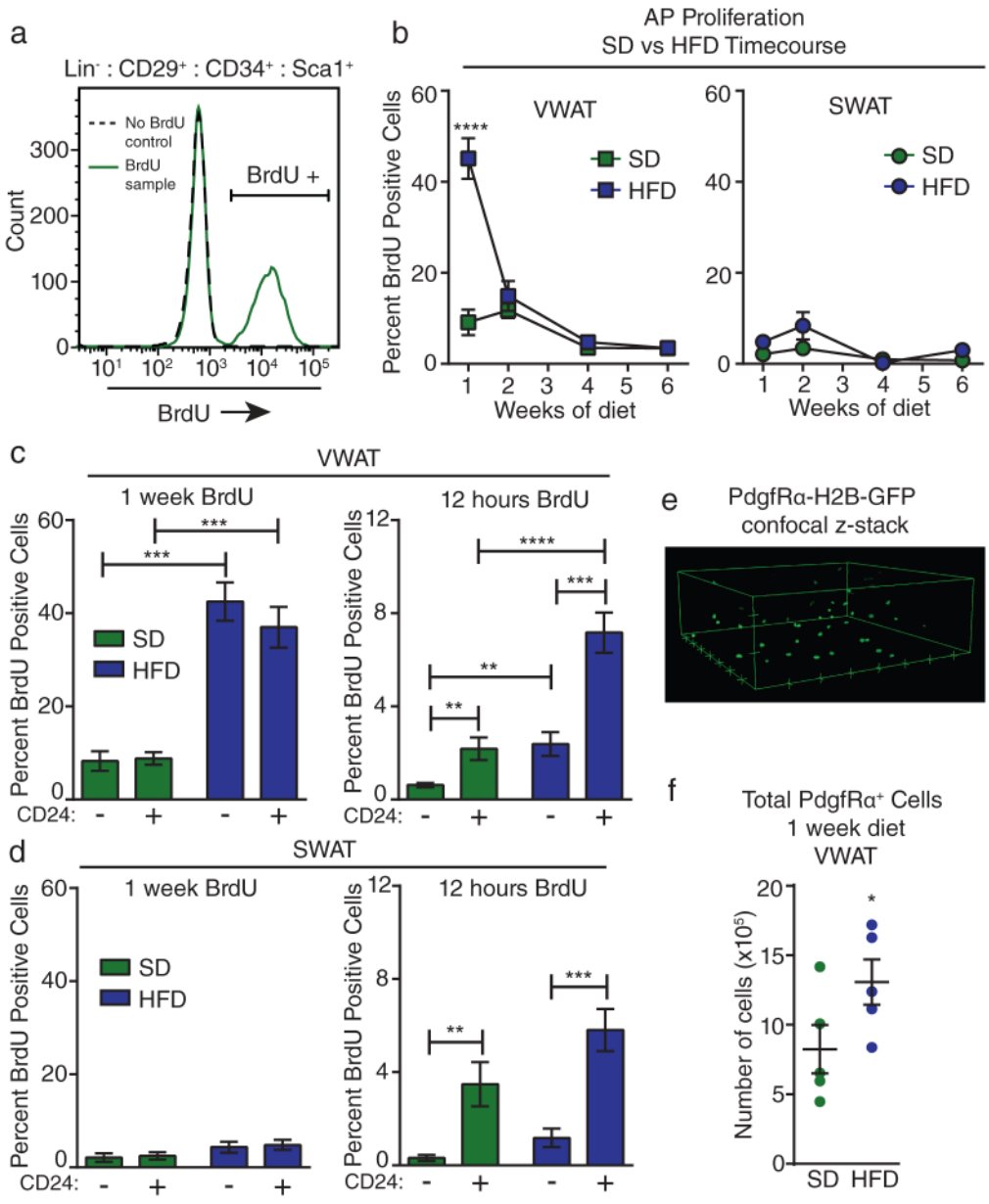

Figure 2. High-fat diet feeding induces adipocyte precursor activation

(**A**) Representative flow cytometry histogram showing gating for BrdU-positive AP cell populations in control (no BrdU treatment) and experimental samples. (**B**) Quantification of BrdU incorporation into APs from VWAT (left) or SWAT (right) of male mice at the indicated time points of diet treatment (see Supplementary Figure 1A). (n = 4 mice for wild-type male SD week 1, n = 5 mice for all other groups). (**C–D**) Quantification of BrdU incorporation into CD24^{+} and CD24^{-} subpopulations of APs in VWAT (C) or SWAT (D) after one week (left panel) or 12 hours (right panel) of BrdU treatment at the onset of HFD feeding compared to SD controls. (For 1 week VWAT n = 4 mice for SD and n = 5 mice for HFD. For 12-hour VWAT n = 10 mice for SD and 7 mice for HFD. For 1 week SWAT n = 4 mice for SD and n = 5 mice for HFD. For 12-hour SWAT n = 8 mice for SD and n = 9

mice for HFD.) (**E**) 3D representation of confocal z-stack from VWAT *of PdgfRα-H2B*-GFP mice showing GFP-positive nuclei. Hash marks represent 50 μm increments. (**F**) Total number of GFP^+ nuclei in the VWAT of *PdgfRα-H2B*-GFP mice after 1 week of HFD compared to SD controls was estimated using confocal microscopy (see methods) (n = 5 mice per group). Significance in (B) was calculated using 2-way ANOVA with Bonferroni's post-test for multiple comparisons. Significance between the indicated groups in (C) and (D) was calculated using a two-tailed student's t-test. Significance in (F) was calculated using a one-tailed student's t-test. Exact p-values are listed in Supplementary Table 1. Statistics source data for 2B can be found in Supplementary Table 2. Error bars represent mean ± s.e.m. * (P<0.05), ** (p<0.01), *** (P<0.001), **** (P<0.0001). AP: adipocyte precursor, HFD: high-fat diet, SD: standard diet, mT/mG: membrane tomato/ membrane GFP; BrdU: bromodeoxyuridine.

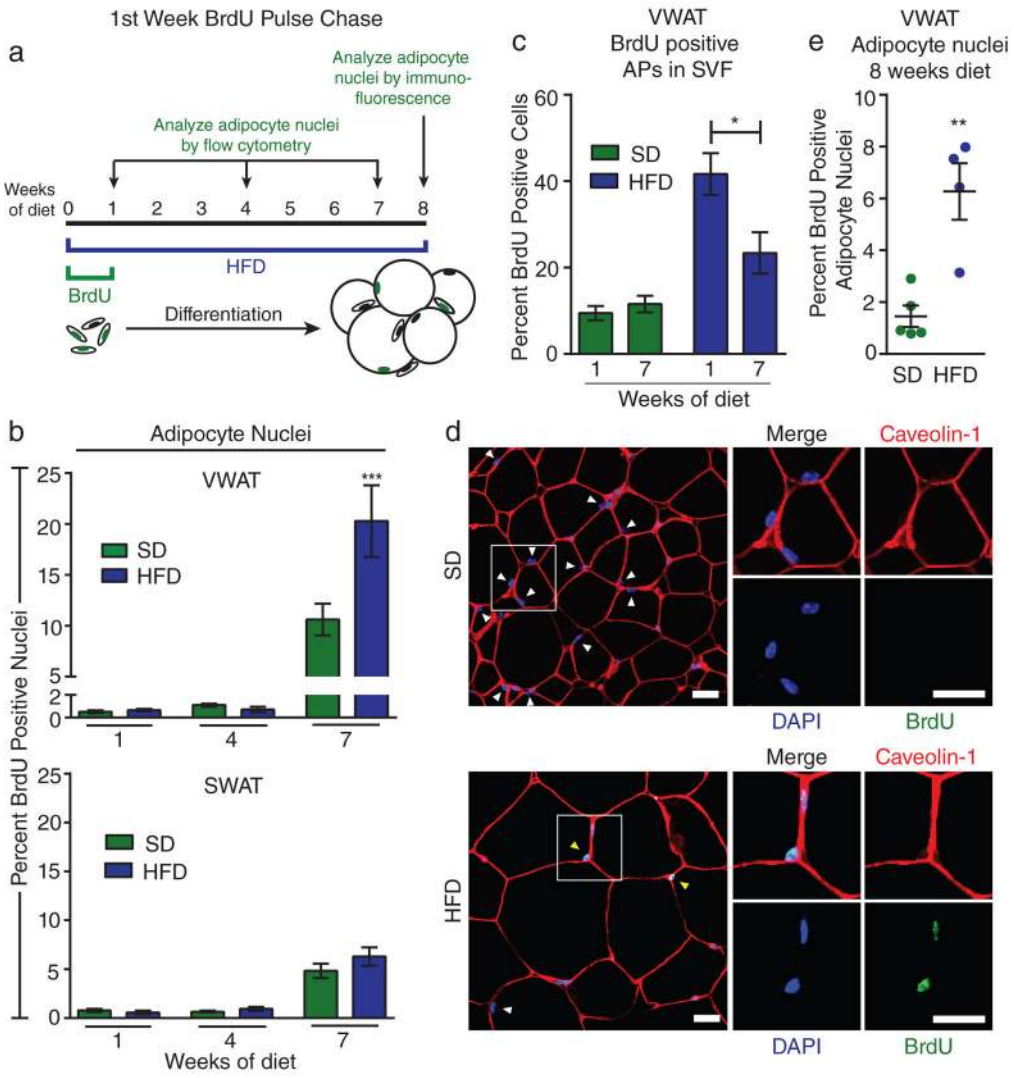

Figure 3. Activated adipocyte precursors undergo adipogenesis in vivo

(**A**) Schematic depicting the time points for BrdU pulse-chase experiments. (**B**) BrdU incorporation into adipocyte nuclei after pulse-chase from the first week of HFD feeding (n = 5 mice for each group) (**C**) Quantification of BrdU incorporation into APs from VWAT of male mice at the indicated time points after BrdU treatment during the first week of diet (n = 5 mice for each group). (**D–E**) Representative images (D) and quantification (E) of immunofluorescence staining for BrdU in adipocyte nuclei of VWAT from mice after 1 week of BrdU treatment and 8 weeks on the indicated diet. Tissue is also stained for caveolin-1 to visualize adipocyte plasma membranes, as well as DAPI to visualize nuclei. Adipocyte nuclei are indicated with arrows (yellow indicates BrdU-positive and white indicates BrdU-negative) are identified by their location inside the adipocyte plasma membrane. Multiple sections were analyzed throughout the VWAT depot. (n = 5 mice for SD, n = 4 mice for HFD) Significance in (B) was calculated using 2-way ANOVA with Bonferroni's post-test for multiple comparisons. Significance between the indicated groups in (C) and (E) was calculated using a two-tailed student's t-test. Exact p-values are listed in

Supplementary Table 1. Error bars represent mean ± s.e.m. * (P<0.05), ** (p<0.01), *** (P<0.001). Scale bars in (D) are 25μm. AP: adipocyte precursor, HFD: high-fat diet, SD: standard diet, BrdU: bromodeoxyuridine.

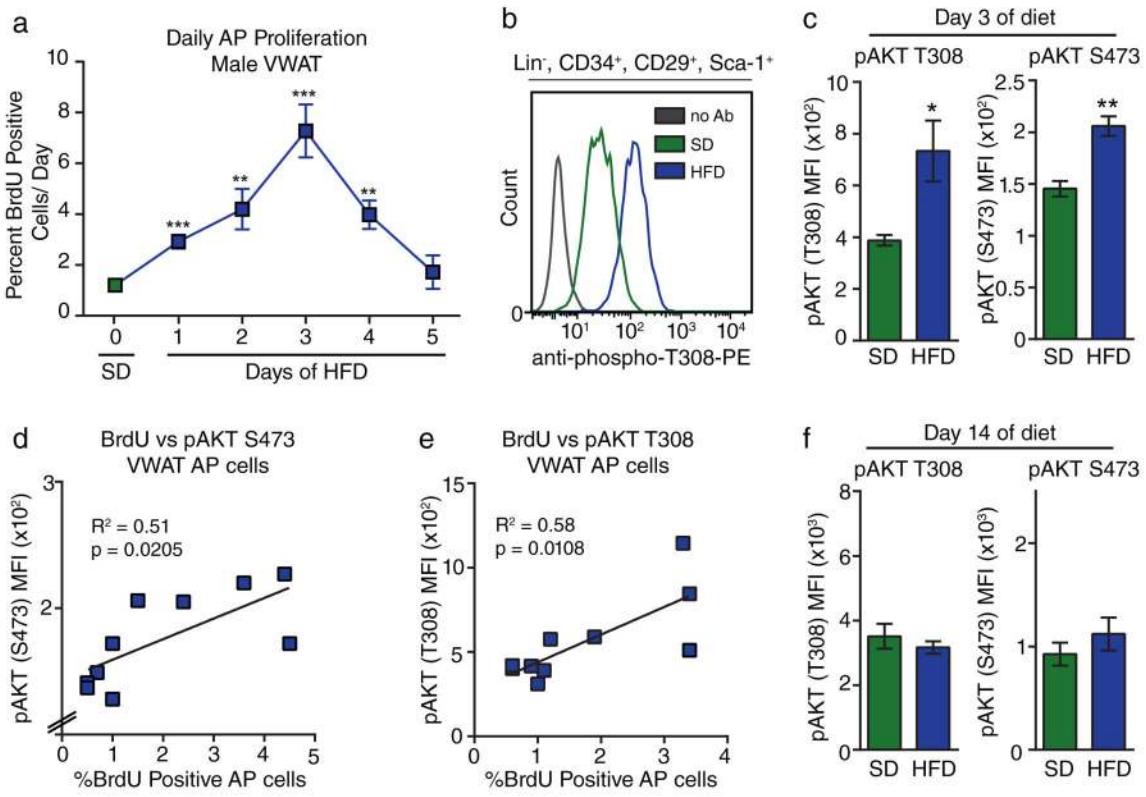

Figure 4. Diet-induced proliferation of adipocyte precursors correlates with cell-intrinsic Akt phosphorylation

(**A**) Quantification of BrdU incorporation into APs from male VWAT after 24-hour pulses of BrdU for each day at the beginning of HFD-treatment. (n = 5 mice for each group) (**B**) Representative flow cytometry histograms of AP stained for phosphorylated AKT (T308) on day 3 of HFD feeding compared to SD and fluorescence-minus one control. (**C**) Quantification of mean fluorescence intensity (MFI) of pAKT staining by flow cytometry in AP cells on day 3 of HFD feeding and SD controls. (n = 5 mice for each group) (**D–E**) Correlation between pAKT T308 (D) or S473 (E) MFI and AP proliferation in VWAT of wild-type mice on day 3 of HFD or SD feeding. (n = 10 mice for each group). (**F**) Quantification of mean fluorescence intensity (MFI) of pAKT staining by flow cytometry in AP cells on day 14 of HFD feeding compared to SD controls. (n = 5 mice for each group) Significance of each HFD group compared to SD in (A) was calculated using a two-tailed student's t-test. Significance in (C) was calculated using a two-tailed student's t-test. Significance in (D) and (E) was calculated using two-tailed correlation analysis. Exact p-values are listed in Supplementary Table 1. Error bars represent mean ± s.e.m. * (P<0.05), ** (p<0.01), *** (P<0.001), **** (P<0.0001). AP: adipocyte precursor, HFD: high-fat diet, SD: standard diet, BrdU: bromodeoxyuridine, pAkt: phosphorylated Akt, MFI: mean fluorescence intensity.

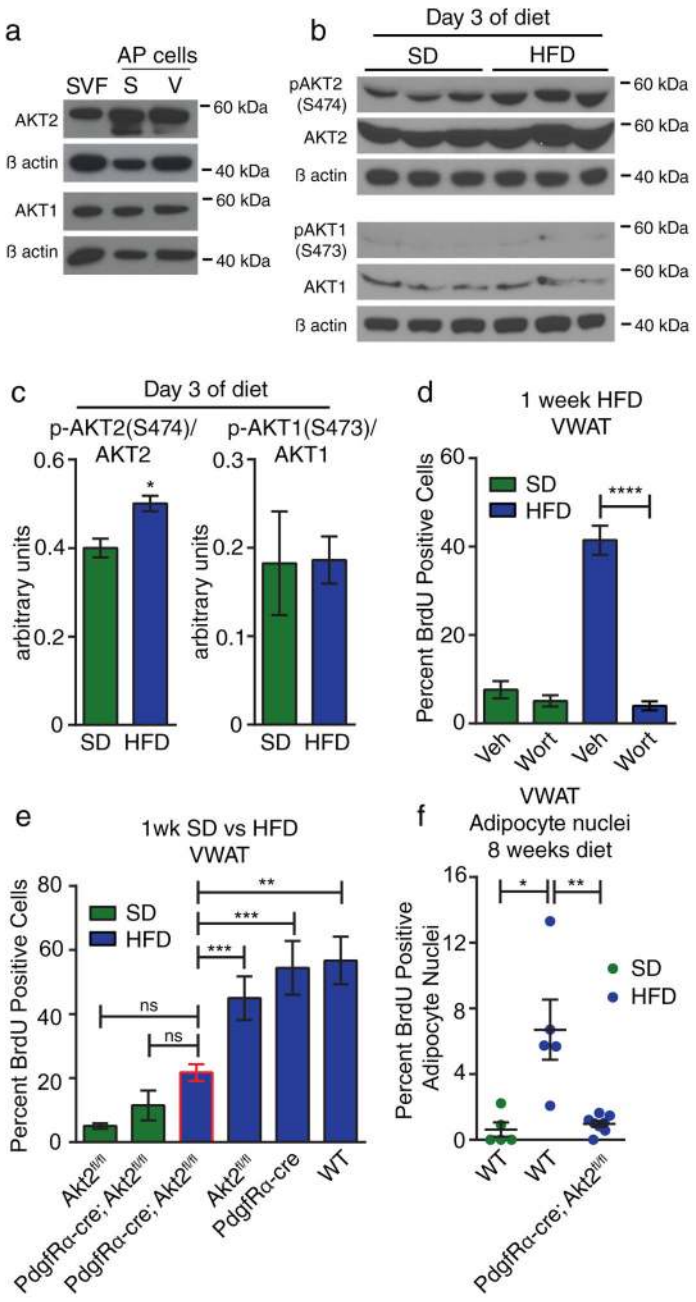

Figure 5. Diet-induced adipocyte precursor activation and adipogenesis requires Akt2 in adipocyte lineage cells

(**A**) Western blot for AKT1 and AKT2 in lysates from SVF or FACS-sorted APs from the SWAT (S) or VWAT (V) depot pooled from 12 wild-type animals. Uncropped blots are shown in Supplementary Figure 7A–B. (**B**) Western blot of lysates from APs enriched from SVF via Sca-1 bead pull down (see methods) after 3 days of HFD or SD. Each lane represents pooled cells from 2 mice. Uncropped blots are shown in Supplementary Figure 7C–H. (**C**) Quantification of western blots in (B) showing normalization of pAKT1 and pAKT2 to total AKT1 and AKT2, respectively. (**D**) Quantification of BrdU incorporation

into VWAT APs after 1 week of HFD or SD with daily injection of wortmannin (Wort), or vehicle (Veh) (n = 5 mice per group). (**E**) BrdU incorporation into VWAT APs of the indicated groups during the first week of HFD feeding compared to SD controls. (n = 7 for *Akt2*$^{fl/fl}$ SD, n = 4 for *PdgfRα-cre; Akt2*$^{fl/fl}$ SD, n = 14 for *PdgfRα-cre; Akt2*$^{fl/fl}$ HFD, n = 8 for *Akt2*$^{fl/fl}$ HFD, n = 5 for wild-type and *PdgfRα-cre* HFD) (**F**) Quantification of immunofluorescence staining for BrdU in adipocyte nuclei of VWAT from the indicated groups of mice after 1 week of BrdU treatment and 8 weeks on the indicated diet. (n = 8 mice *for PdgfRα-cre; Akt2*$^{fl/fl}$ HFD, n = 5 mice for wild-type groups). Significance between the indicated groups in (C), (D), and (F) was calculated using a two-tailed student's t-test. Significance in (E) was calculated using one-way ANOVA with Tukey's test for multiple comparisons. Exact p-values are listed in Supplementary Table 1. Statistics source data for 5C can be found in Supplementary Table 2. Error bars represent mean ± s.e.m. * ($P<0.05$), ** ($p<0.01$), *** ($P<0.001$), **** ($P<0.0001$). SVF: stromal-vascular fraction, AP: adipocyte precursor, HFD: high-fat diet, SD: standard diet, BrdU: bromodeoxyuridine, Veh: vehicle, Wort: wortmannin.

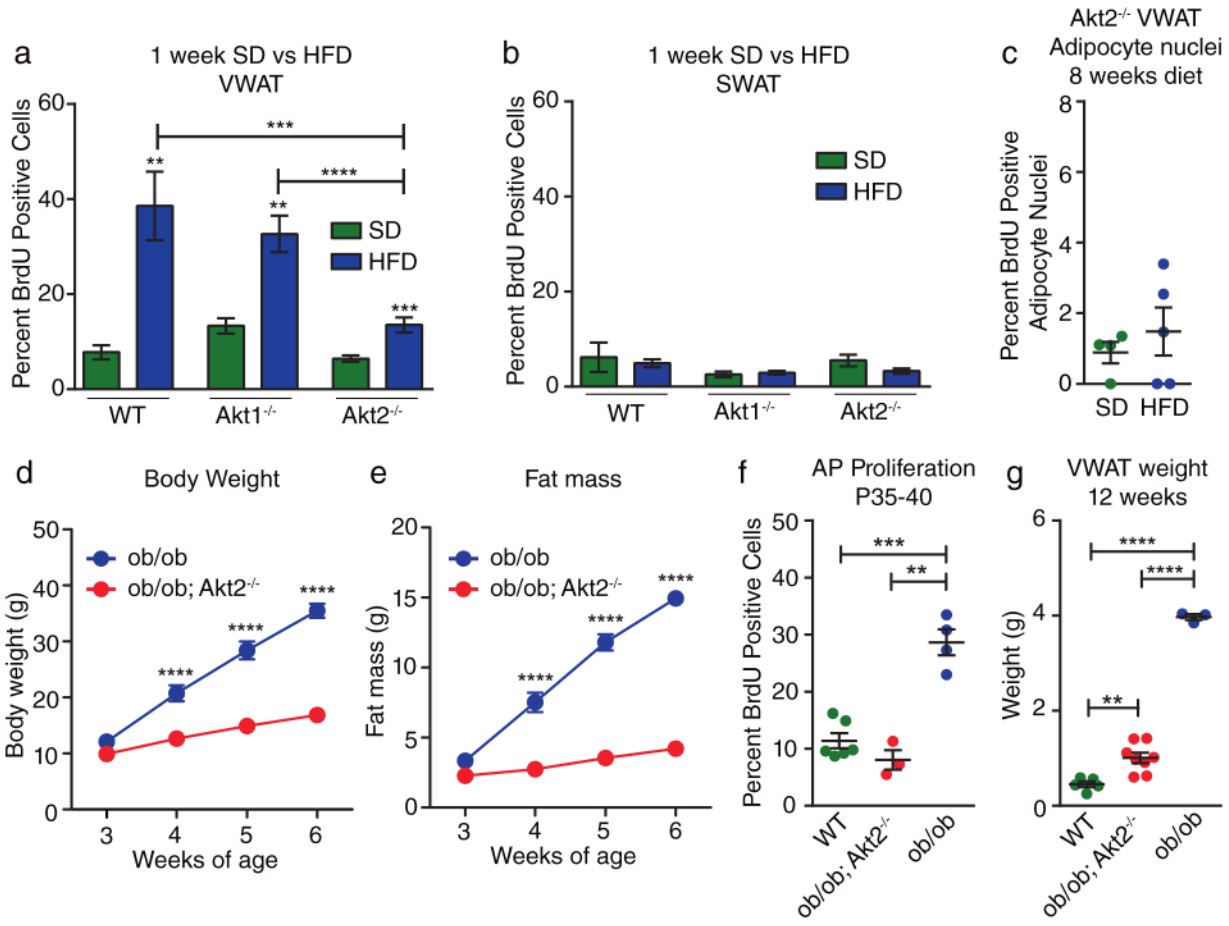

Figure 6. AKT2 is required for activation of adipocyte precursors in multiple models of obesity

(**A–B**) BrdU incorporation into VWAT (A) or SWAT (B) APs of the indicated groups after 1 week of treatment. (n = 5 mice for wild-type SD, n = 7 mice for wild-type HFD, n = 6 mice for *Akt1*$^{-/-}$ SD, n = 7 mice for *Akt1*$^{-/-}$ HFD, n = 17 mice for *Akt2*$^{-/-}$ SD, n = 15 mice for *Akt2*$^{-/-}$ HFD.) (**C**) Quantification of immunofluorescence staining for BrdU in adipocyte nuclei of VWAT from *Akt2*$^{-/-}$ mice after 1 week of BrdU treatment and 8 weeks on the indicated diet. (n = 4 mice for SD, n = 5 mice for HFD). (**D–E**) Body weight (D) and fat mass (E) in young mice after weaning at 3 weeks of age. (n = 7–8 mice for *ob/ob; Akt2*$^{-/-}$, n = 4 mice for *ob/ob*). Some error bars are obstructed by symbols. (**F**) BrdU incorporation into VWAT APs in the indicated groups after BrdU treatment from P35–40. (n = 6 mice for wild-type, n = 4 mice for *ob/ob* and n = 3 mice for *ob/ob; Akt2*$^{-/-}$). (**G**) VWAT weights of the indicated groups at 12 weeks of age. (n = 5 mice for wild-type, n = 8 mice for *ob/ob; Akt2*$^{-/-}$, n = 3 mice for *ob/ob*). Significance between indicated groups in (A–C) was calculated using a two-tailed student's t-test. Significance between indicated groups in (D–E) was calculated using 2-way ANOVA with Bonferroni's post-test for multiple comparisons (p-values are adjusted p-values). Significance in (F–G) was calculated using a two-tailed student's t-test. Exact p-values are listed in Supplementary Table 1. Statistics source data for 6D–E can be found in Supplementary Table 2. Error bars represent mean ±

s.e.m. * (P<0.05), ** (p<0.01), *** (P<0.001), **** (P<0.0001). AP: adipocyte precursor, HFD: high-fat diet, SD: standard diet, BrdU: bromodeoxyuridine.

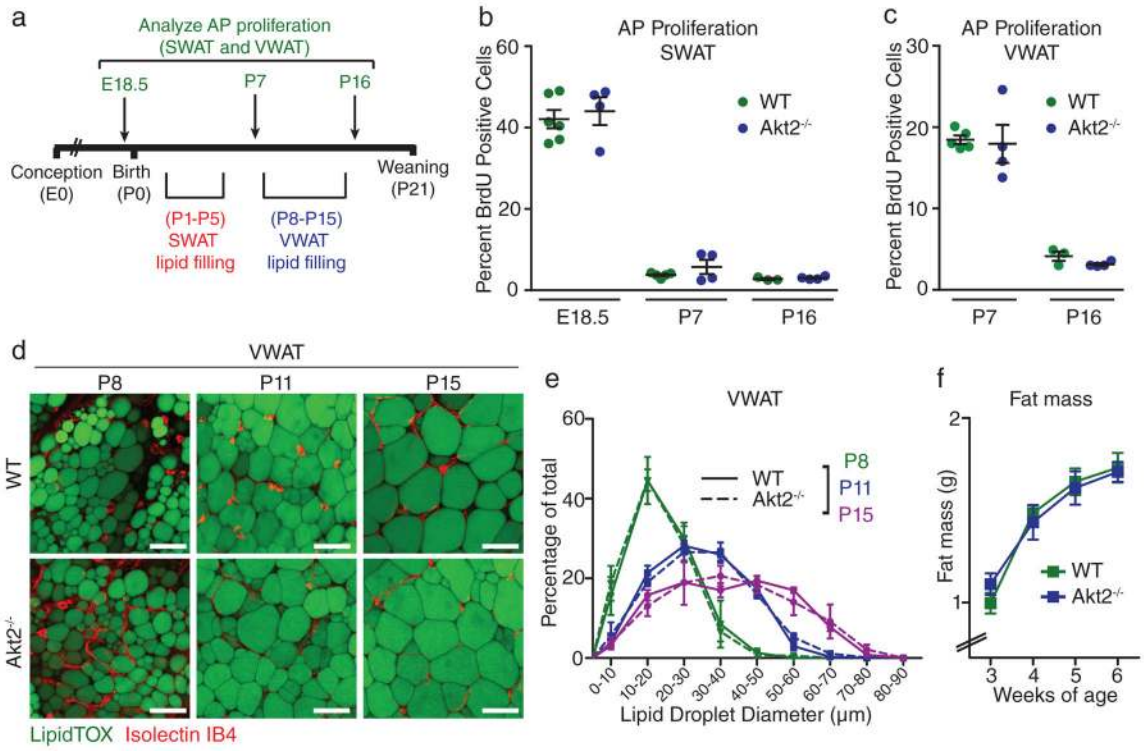

Figure 7. AKT2 is not required for normal development of white adipose tissue

(**A**) Schematic depicting the time points when the indicated experiments were performed during WAT development. (**B–C**) Quantification of BrdU incorporation into APs of SWAT (A) and VWAT (B) after 24-hour BrdU treatment at the indicated days of embryonic (E) and postnatal (P) development in wild-type and *Akt2*$^{-/-}$ mice. (n = 6 mice for wild-type E18.5, n = 5 mice for wild-type P7, n = 3 mice for wild-type P16, n = 4 mice for *Akt2*$^{-/-}$ groups). Each group represents a single litter. All mice are male except mice in the E18.5 group, for which male and female data are combined (**D–E**) Confocal images (D) of developing wild-type and *Akt2*$^{-/-}$ VWAT stained with LipidTOX (a lipid stain) and Isolectin IB4 (an endothelial cell stain) and (E) corresponding lipid droplet size quantification based on LipidTOX staining (n = 3 mice for P8 and P15, n = 4 mice for P11). Each group includes mice from 2 different litters, except *Akt2*$^{-/-}$ P11, which contains mice from 3 litters. (**F**) Echo MRI analysis of fat mass throughout development in wild-type and *Akt2*$^{-/-}$ mice. n = 13 mice except for wild-type week 5 (n = 18 mice), wild-type week 4 (n = 14 mice), *Akt2*$^{-/-}$ week 5 (n = 11 mice), and *Akt2*$^{-/-}$ week 6 (n = 10 mice). wild-type mice are from 4 different litters. *Akt2*$^{-/-}$ mice are from 6 different litters. Error bars represent mean ± s.e.m. Scale bars are 50μm in (D), AP: adipocyte precursor, BrdU: bromodeoxyuridine.